Effect of Antenna and Array Positioning on Microwave Bladder State Detection

Andrew Fry, *Student Member, IEEE*, Cameron Jeffery, Alan Poisot Palacios, Eleonora Razzicchia*, Member, IEEE,* Laura Estep, and Emily Porter, *Member, IEEE*

***Abstract*— Microwave sensing technologies have the potential to be used to non-invasively monitor bladder volume to support toilet training for children with autism spectrum disorder and/or intellectual and developmental disabilities. Importantly, these technologies are relatively low-cost with low-form factor, and safe for 24/7 usage. In this work, we study the impact and importance of antenna placement on the pelvic region to robustly discriminate the full bladder state for the first time. A series of studies are conducted to determine the relative importance of antenna positions in different locations relative to the bladder, and the relative spacing between elements in an array, to maximize detectability of bladder state.**

***Index Terms*—Antenna Arrays, Bladder, Microwaves, Monitoring, Toilet Training Support, Urinary Incontinence**

I. Introduction

URINARY incontinence (UI) is a widespread condition that significantly impacts individuals' autonomy, dignity, and overall health. It is estimated that 25-45% of the worldwide population is affected by UI: this includes individuals with autism spectrum disorder (ASD), intellectual and developmental disabilities (IDD), neurological conditions (e.g., multiple sclerosis, Parkinson's disease, stroke, brain tumors, and spinal cord injuries), and the elderly. UI negatively impacts quality of life both physically and psychologically. Physically, it can lead to skin irritation, increased risk of urinary tract infections (UTIs), and in severe cases, kidney damage. Psychologically, individuals may experience stress, guilt, shame, humiliation, and depression [1] [2] [3] [4] [5] [6] [7] [8] [9].

In this work, we focus on a particularly vulnerable group facing significant challenges in this area: children with ASD/IDD. These children often have delayed onset of toilet training [5] [10] [11], which, if unaddressed, may continue into youth and adulthood [10] [11], limiting access to community settings and integration with their peers. More than 2% of children in the U.S. are diagnosed with ASD/IDD, accounting for more than 500,000 children and 5 million adults affected [12] [13] [14]. Children with ASD/IDD often have difficulty with toilet training due to not recognizing the sensation of a full bladder, and/or not being able to respond appropriately in a timely manner [15] [16] [17].

There are many varied approaches to treating UI and/or supporting individuals with UI. These approaches depend on each individual's specific condition as well as their physical and mental health status. Management methods include pharmaceutical treatment and behavioral strategies; however, these approaches are broadly under-effective [1] [15] [18] [19] [20] [21] [22]. Technological support tools are also used to manage or monitor UI, and to provide toilet training support. Devices may be invasive or non-invasive.

Non-invasive management methods for children with ASD/IDD include the use of diapers, wetness sensors, and other technological supports such as timers or video examples, but these fail to help the child learn to understand their body's signals as they do not account for individualized bladder filling rates [1] [20] [23] [24] [25]. Invasive solutions such as catheters are typically avoided for children where possible, and they do not support toilet training.

In the last several years, technology-based non-invasive bladder monitoring methods including ultrasound (US), electrical impedance tomography (EIT), and near-infrared spectroscopy (NIRS) [25], have been developed and may eventually support toilet training. US for bladder monitoring has recently entered the market via the SENS-U by Novioscan in the Netherlands [26] [27]. However, while showing promising performance in research, it is generally more expensive than the other options and requires gel for proper

This paragraph of the first footnote will contain the date on which you submitted your paper for review, which is populated by IEEE.

This work was supported by the National Institute Of Nursing Research of the National Institutes of Health (Award Number 1R21NR020653-01A1). The content is solely the responsibility of the authors and does not necessarily represent the official views of the National Institutes of Health. The work was further supported by McGill University's Faculty of Medicine and Health Sciences and the McGill University Health Centre Foundation start-up funds.

A. Fry is with the Chandra Family Department of Electrical and Computer Engineering at The University of Texas at Austin, 2501 Speedway, Austin, TX 78712, USA (atfry@utexas.edu).

C. Jeffery A. Poisot Palacios, E. Razzicchia and E. Porter are with McGill University, and the Cancer Research Program of the Research Institute of McGill University Health Centre, 3775, rue University, Montréal, QC H3A 2B4, Canada ({cameron.jeffery, alan.poisotpalacios, eleonora.razzicchia}@mail.mcgill.ca, emily.porter@mcgill.ca).

L. Estep is with the Department of Special Education at The University of Texas at Austin, 1912 Speedway, Austin, Texas 78712, USA (laura.estep@austin.utexas.edu).

Color versions of one or more of the figures in this article are available online at http://ieeexplore.ieee.org

performance [25]. EIT technologies strike a balance between cost and accuracy compared to NIRS and US. The recent developments in integrating EIT into wearable (fabrics, not just adhesive) technology have made way for EIT to become a viable market option, but more research is needed to address concerns with reliability and consistency of measurements [25]. NIRS, while affordable, has had lower accuracy than EIT and US [25]. Less NIRS research work in general has been done on this topic, but recently, a mix of NIRS sensors on the abdomen and brain has shown promise in research [28]. Despite their promise, none of these approaches have found widespread clinical acceptability to date due to various limitations, and, importantly, none are used as part of the standard of care in supporting people with toileting issues.

A recently proposed alternative option for bladder monitoring, microwave (MW) technologies, is promising due to affordability, non-invasive nature, good penetration depth in the body, and potential for integration into wearable devices [8] [29] [30]. It is expected that MW bladder monitoring technologies will have similar benefits as EIT, but with better penetration depth and resolution. Notably, MW sensing technologies are also safe for continuous, 24/7 exposure [31] [32] [33] [34]. However, MW technologies are just emerging for this application. The purpose of this work is to lay the groundwork to develop an affordable MW bladder monitoring technology to provide an alert to the child or carer when it is time to go to the toilet. Such a solution would avoid accidents and all of the associated clean up, while also supporting children in learning to recognize and act on the sensation of fullness proactively.

To date, MW bladder monitoring technologies have been simulated in bladder models ranging from highly simplified layered models to MRI-derived body structures [8] [30] [35] [36] [37] [38] [39] [40] [41] [42] [43]. However, no studies have examined the effect or importance of relative antenna positioning in an array, which is central to achieving robust bladder state measurements. Therefore, in this work, we study the effect of antenna and array positioning on bladder fullness detection using MW for the first time. We note that we particularly focus on an antenna array that can be conformed to the skin, for ease in adaptability to wearable usage.

II. Methods

In this section, the design of an anatomically and dielectrically representative pelvic bladder model is introduced, followed by descriptions of the antennas, simulation set-up, and test scenarios investigated. Lastly, the various analyses are detailed.

A. Pelvic Model Design

Studies to date on this topic have used simplified elliptical or rectangular layered models which do not fully encapsulate the complexity of the pelvic region [8] [35] [37] [38] [39] [40] [41] [42] [43] or have used models developed from full body imaging which were highly complex, and as a result, not computationally feasible [8] [30] [36].

Therefore, a pelvic model that strikes a balance between computational simplicity and anatomical accuracy was developed in our recent work [44] and is summarized here. Importantly, this model allows for anatomical realism in a manner that still enables computational simulation of the interacting electromagnetic fields.

The bladder is modeled as a triaxial ellipsoid filled with urine. When full, the top of the bladder model is tilted towards the front of the body to capture how the bladder shape changes as it fills. Assuming there is always some residual urine volume, the bladder volumes when empty and full are 23 mL and 300 mL, respectively as reported in [44].

The bone structure is composed of the sacrococcygeal area and pelvic bone/inlet. The sacrococcygeal area is created by intersecting an angled, truncated cone with a bent rectangular prism. The labeled model can be seen in Figs. 1 and 2, and the dimensions can be seen in Table I. Fig. 3 Shows the full and empty pelvic models. The muscle layer is assumed to maintain a similar shape to the bone structure, while the skin and fat will expand to fill the model. The model represents an average human, and size was determined from the NHANES database. The model is described in more detail with parameter justifications in [44].

The tissue surrounding the bone is estimated as a mixture of fat and muscle based on a fat-to-muscle mass ratio of 0.4:1. This ratio was chosen based on the dielectric properties of internal organs, a representative fat-to-muscle ratio in healthy individuals, and the anatomical volume distribution of organs in the pelvic region [45] [46] [47]. Bruggeman's effective medium approximation is used to calculate the dielectric properties for the mixed tissue area. The frequency-dependent dielectric properties were obtained from [45] and are summarized in Table II at 3.7 GHz.

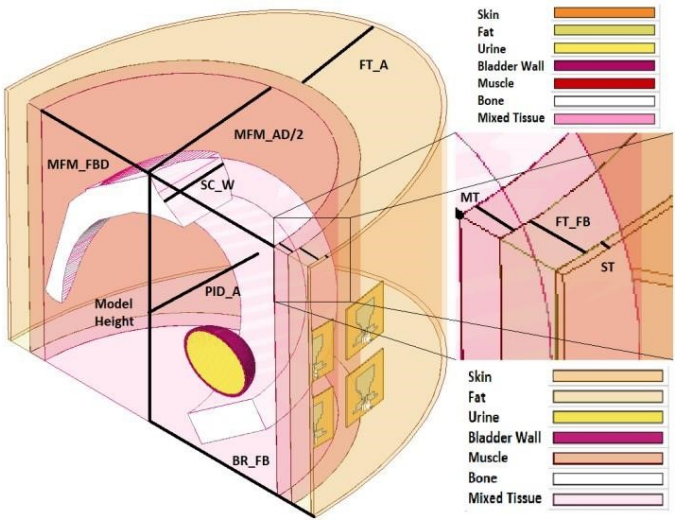

Fig. 1. Balcony view of empty bladder model with cut plane. The legend on the bottom right shows the tissue colors as they appear with transparency on in the model. The legend in the top right shows the tissue colors as solids *[44]*.

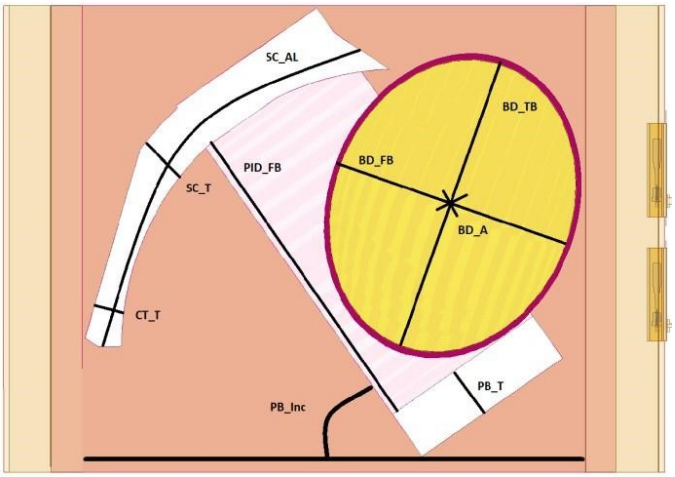

Fig. 2. Side view of full bladder model with cut plane. On the right-hand side, the side view of two antennas in contact with the skin layer can be seen *[44]*. The colors of the tissues are as presented in Fig. 1.

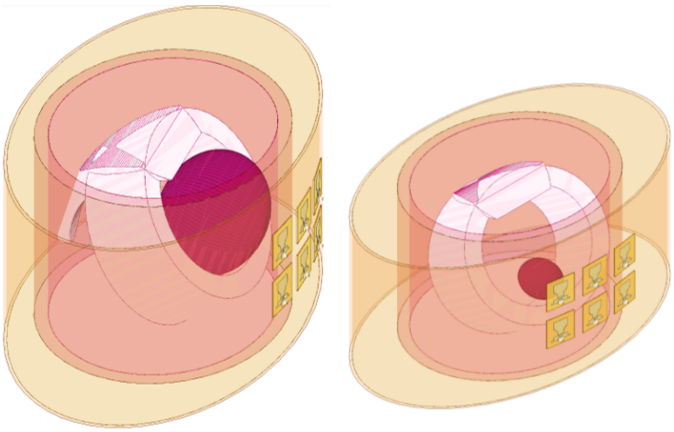

Fig. 3. The entire full (left) and empty (right) pelvic region models shown at trimetric and isometric angles respectively with a 6-antenna array on the skin.

TABLE I
BLADDER MODEL DIMENSIONS

Variable	Length (mm)	Variable	Length (mm)
Bladder Wall Thickness	3.15	BD_A (full)	80
Model Height	150	BD_A (empty)	18.5
Model Circumference	880	BD_TB (full)	100
MFM_FBD	81	BD_TB (empty)	17.5
MFM_AD	95.5	SC_W	88
MT	10	SC_AL	165
ST	2	SC_T	15.5
FT_FB	13.5	CT_T	10
FT_A	62.5	PB_T	16.5
BR_FB	106	PID_FB	105
BD_FB (full)	80	PID_A	130
BD_FB (empty)	22	PB_Inc	55 (°)

TABLE II
ASSIGNED TISSUE DIELECTRIC PROPERTIES AT 3.7 GHZ

Tissue	Relative Permittivity	Conductivity (S/m)
Skin	36.8	2.15
Fat	10.4	0.45
Muscle	51.2	2.74
Mixed	34.0	1.76
Bone	9.66	0.70
Bladder Wall	17.4	1.06
Urine	66.9	4.01

B. Antenna Designs

Two antennas are explored in this work: a Vivaldi antenna that has high directivity (potentially enabling a strong response from the bladder) but that would require a bulky antenna array and support structure; and, a conformal patch antenna with broadband radiation that is good for wearability but with a non-directional wide radiation pattern.

The Vivaldi antenna is implemented first, as it is expected to be able to readily monitor the bladder. However, it is not suitable for a wearable applications. This first simulation study aims to confirm the feasibility of MW bladder state detection with an antenna type which is already well-established for MW sensing in other biomedical applications, and has shown promise for bladder sensing in simplified models [8] [37] [38] [39] [40] [41] [42] [43] [48]. This study represents the first simulation of a Vivaldi antenna on an anatomically representative complex model. This end-fire antenna measures 60 x 60 mm^2 with geometry as described in [49] and a matching medium as described in [50]. An S_{11} < - 10 dB on the skin of the pelvic region over the frequency range of interest was confirmed. Simulations are conducted for one antenna only, positioned at different heights on the pelvic region, to demonstrate the discrimination potential between full and empty bladders.

Next, a flexible, conformal, stepped monopole antenna with broadside radiation described in [51] is implemented. The broadside radiation with conformal design makes this antenna ideal for a wearable, which is the end goal for regular bladder monitoring. However, the non-directive radiation may result in lower-amplitude signals and more challenging discrimination of bladder volume. The substrate of the antenna (30 mm x 30 mm) is Kapton polyimide. The S_{11} frequency response was confirmed to be less than -10 dB on the pelvic region. For this antenna, several scenarios are studied, with 2-6 antenna elements on body in different positions to study the optimal number and relative positioning of antennas (scenarios are detailed in Section II.D).

C. Simulation Setup

Full wave 3-D electromagnetic simulations were performed using Ansys HFSS. For all simulations, the maximum delta S (convergence condition) was set to 0.001. The mesh settings used auto for the mesh method with the option to apply curvilinear meshing to all curved surfaces enabled. Curved surface meshing was performed using dynamic surface resolution, with the slider set to the “fine” level.

Three high-level types of simulations were performed: i) with the Vivaldi antenna; ii) with a 2-element array of monopoles; and iii) with a 6-element array of monopoles. The frequency range was 0.5 - 4 GHz with 201 evenly spaced (17.5 MHz) for the Vivaldi, 3.3 - 4.1 GHz with 21 evenly spaced (40 MHz) frequency points for the 2-element monopole, and 1- 5 GHz with 81 evenly spaced (50 MHz) frequency points for the 6-element (test scenarios are described in detail in Section II.D). The 6-element array was simulated with maximum considered

spacing in x and y directions, then the model was cut to the -50 dB E-field level.

For a 6-element monopole array, simulations took around 8 hours and 6 hours to run for full and empty, respectively, while 2-element simulations took around 2 hours per permutation for both empty and full utilizing the Texas Advanced Computing Center (TACC) supercomputers. The single antenna Vivaldi simulations took around 4 hours per permutation while utilizing the supercomputing resources provided by CMC Microsystems and the Digital Research Alliance of Canada.

D. Simulation Test Scenarios

First, the Vivaldi antenna is simulated, as shown in Fig. 4. A vertical sweep is performed with a single antenna at Y coordinates of 23.5 mm, 43.5 mm, and 63.5 mm, to establish the ability to discriminate full and empty bladder volumes with a highly directional antenna.

Next, in order to study the effect of antenna placement for MW bladder monitoring, three scenarios are explored with the conformal monopole antenna. A visual schematic of these scenarios is presented in Fig. 5. The first two scenarios together facilitate the study of antenna placement effects in the horizontal and vertical planes relative to the bladder, while the third demonstrates the added utility of a 6-element array.

Scenario 1: To study the effect of antenna placement in the vertical direction on the ability to discriminate bladder fullness, a two-part, 2-element vertical antenna sweep is performed where the 2 antennas are placed on the center of the model. First, Y_b, the Y coordinate of the bottom antenna, is held at Y = 25 mm while Y_t, the Y coordinate of the top antenna, is swept downward from Y = 75 mm to Y = 45 mm (where the substrates touch) in 5 mm increments. Then, Y_t is held at Y = 75 mm while Y_b is swept upward from Y = 25 mm to 45 mm in 5 mm increments. This sweep results in 9 unique antenna placements, and the held positions are based on the best responses from initial simulations where a full row of antennas were vertically swept from Y = 0 mm to Y = 80 mm.

Scenario 2: To examine how horizontal antenna positioning affects the ability to discriminate bladder fullness, a 2-element horizontal sweep is performed where the antennas are held at Y = 75 mm based on the results of the vertical sweep. X_R, the X coordinate of the right antenna, is held at the center, X = 0 mm, while X_L, the X coordinate of the left antenna is swept from X = -40 mm to -80 mm in 10 mm increments for 5 pairs of antenna placements. Appropriate depth and angle adjustments are made to keep the sweeping antenna conformal with the skin.

Scenario 3: To investigate the impact of additional antennas on the ability to discriminate bladder state, the results of Scenarios 1 and 2 are analyzed to choose the antenna locations for a 6-element antenna array, composed of 2 rows of 3 elements each. A 6-element array is chosen to effectively cover the area the bladder expands into, while allow proper spacing of the antenna elements.

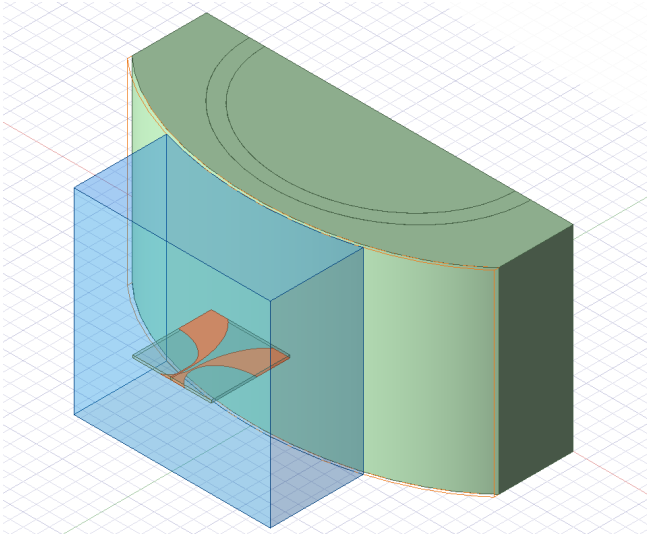

Fig. 4. The pelvic model with a Vivaldi antenna immersed in the matching medium in perpendicular contact with the skin of the pelvic model.

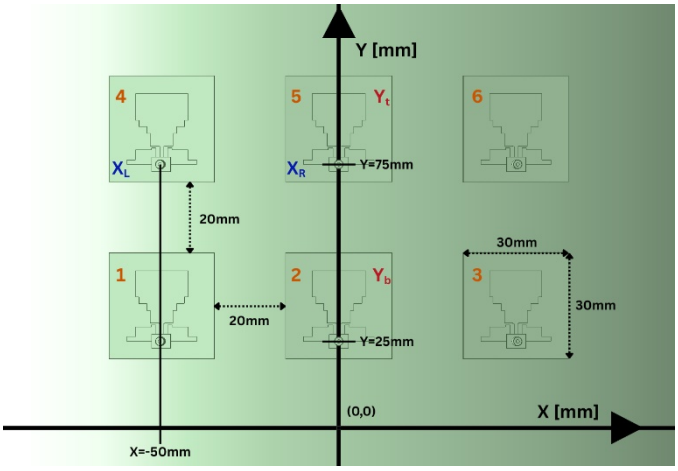

Fig. 5. Labeled 6-element monopole antenna array on the pelvic region model, using 20 mm spacing as applied in Scenario 3. The top left labels (orange) on the antennas indicate their element indices. The labels on the top right (red) of antennas 2 and 5 denote their use in the vertical sweep (Scenario 1) and specify the corresponding coordinate variables. The labels on the bottom left (blue) of antennas 4 and 5 indicate their roles in the horizontal sweep (Scenario 2). Y = 0 is centered on the section of the pelvic bone structure that is closest to the skin and intersects with X = 0, the center of the model in the X-direction. The dimensions of the antennas are labeled on antenna 3.

E. Data Analysis

For the Vivaldi antenna, changes in S-parameters between full and empty bladder are studied to establish the detectability of a full bladder state. For the antenna placement studies conducted with the conformal monopole antennas, results were analyzed through three different approaches to provide complementary perspectives on the ability to discriminate full vs. empty bladder and to assess optimal element locations, relative positions, and/or numbers.

1) Raw S-Parameter Differences:

For each simulation of each scenario, the complex frequency-dependent S-parameters were exported from Ansys HFSS for analysis in MATLAB. The differences in S_{ii} and S_{ij} parameters between full bladder and empty bladder, at each frequency point, were calculated.

2) Mutual Information Coefficients:

In order to quantitatively characterize the differences in information obtained from various antenna positions (for the 2-element sweeps) or from different antenna elements (6-element array), a mutual information coefficient (MIC) was calculated via:

$$\mathrm{MIC}(i,j) = \frac{\left|\sum_f S_i(f)\cdot S_j^*(f)\right|}{\sqrt{\sum_f |S_i(f)|^2 \cdot \sum_f |S_j(f)|^2}}, \quad (1)$$

where i and j are the indexes of the antennas ($i \neq j$), and $S(f)$ represents all of the transmission parameters (S_{ij}) in complex form that include the respective antennas [52].

However, to compare the different locations for the 2-element sweeps, the equation is modified such that i and j are assigned as the swept antenna locations, and $S(f)$ can include any or all of the S-parameters (i.e., reflection or transmission) for both permutations. To include multiple S-parameters in the calculation, they are concatenated into a single array. For pair ordering in the antenna element MIC calculation, transmission S-parameters with the same coupled antenna should be used. For example, when calculating the MIC between antennas 1 and 3, S_{12} should be paired with S_{32} and S_{16} with S_{36}.

The output for the MIC is a range from 0 to 1 where 1 indicates that the information gained from the different scenarios or antenna elements are completely redundant, while lower numbers indicate more unique information gained. Heatmap matrices of MIC are created for analysis of each simulation scenario.

3) Radar-based Image Reconstruction:

The Microwave Radar-based Imaging Toolbox (MERIT) was used to reconstruct radar images [53]. Images are reconstructed from backscattered signals collected across multiple channels within a defined region. By combining and summing the signals from all channels, it generates an energy profile that highlights areas of significant dielectric contrast. The algorithm processes frequency-dependent, complex-valued S-parameters.

In this work, images were only reconstructed with data from the 6-element antenna array. 3-D imaging of the pelvic region was performed on the full bladder with the empty bladder signals used as the reference scan. The MERIT algorithm assumes a homogeneous media, and the input relative permittivity was set to 19.72 as it is estimated to represent the average permittivity of tissues in front of the antenna array.

III. Results

In this section, simulation data analysis is presented as described in Section II.E for each study. First, the results for Vivaldi antenna study are presented followed by the 2-element positioning study then the 6-element array study.

A. Vivaldi Antenna: Feasibility Test of MW Bladder Discrimination

Fig. 6 displays a comparison between the reflection S-Parameters obtained for each antenna height for both full and empty bladder models. The inset graph shows that there are substantial changes between the signals obtained from the full and empty bladder models, which are readily detectable as they can reach more than 20 dB. These results support the ability to detect the bladder state with the use of antennas operating in the MW range, especially with a highly directive antenna operating at low frequencies between 0.5-1.5 GHz.

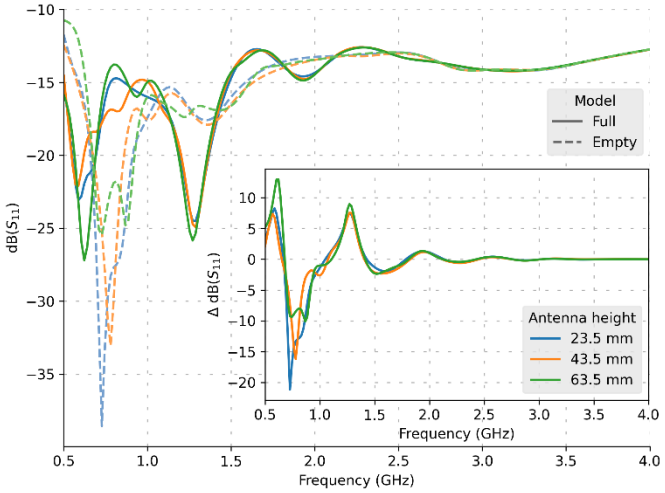

Fig. 6. S_{11} magnitude vs frequency plot for each pelvic region model (full and empty) and antenna height (23.5 mm, 43.5 mm, and 63.5 mm). The inset plot shows the difference between the S_{11} magnitude of the full and empty models, for each antenna height.

B. Two-Element Positioning Study

1) Raw S-Parameters:

Fig. 7 provides an example of each S-Parameter with numerical error included from the Scenario 1 permutation with Y_b = 25 mm, Y_t = 55 mm. Note that there is an evident difference between the full and empty data, even with error, for both reflection parameters despite this permutation having one of the lowest differences in signal between empty and full out of the set. Also, note that for the reflection coefficients, the full signal level is always higher than the empty signal level in every permutation (Scenario 1 and 2) of the simulations. The opposite is true for the transmission coefficients where the empty signal level is always higher than the full signal level.

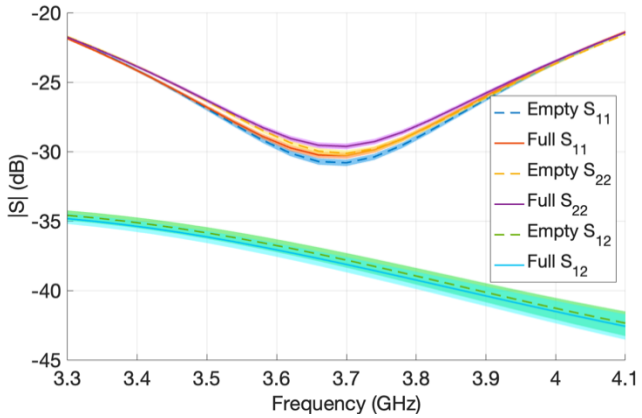

Fig. 7. Raw S-Parameter magnitude vs frequency plot for Y_b = 25 mm, Y_t = 55 mm from Scenario 1. All S-Parameters are included. The shaded regions show the numerical error based on the convergence reached in the simulation and the signal level at each frequency point.

2) Difference Graphs:

Figs. 8-12 plot the difference in S-parameters between full and empty bladder for various scenarios. Figs. 8 and 9 both indicate that the highest difference is at the Y_b = 25 mm, Y_t = 75 mm permutation from Scenario 1. When only considering the location of the bladder between empty and full, it is expected that the reflection coefficient difference would be more pronounced with higher Y_b and lower Y_t, but that is not the case (except for Y_b = 45 mm). This indicates that when multiple antennas are included in the sensing system, the spacing between elements plays an important role, not just location. When studying Fig. 10, it appears that higher differences occur in the transmission coefficients when there are lower differences in the reflection coefficients. This insight could be used to inform the design of an asymmetrical antenna array. The maximum differences for the reflection coefficients occur within the resonance range around 3.7 GHz, which is expected since this is where the most signal penetrates into the object under test. The maximum differences in transmission coefficients occur at higher frequencies, likely due to a combination of lower signal levels and more pronounced dielectric property variations at those frequencies. Regarding phase differences, these remain relatively consistent across the frequency range; however, the maximum phase difference typically occurs at a slightly lower frequency than the resonance for the reflection coefficients. For the transmission coefficients, the maximum phase difference frequency shifts depending on the spacing between the antennas and is also relatively consistent across frequency range.

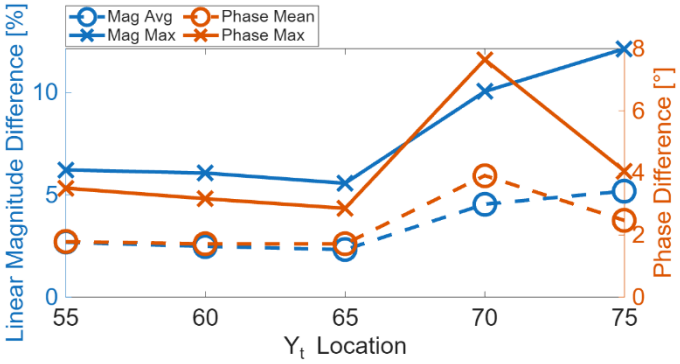

Fig. 8. Full vs empty difference plot of the reflection coefficient for antenna 5 as it sweeps across Y_t while Y_b is held at 25 mm. The average signal at the points of maximum magnitude difference is -30.16 dB, occurring at 3.71 GHz on average. The maximum phase differences occur at 3.55 GHz on average.

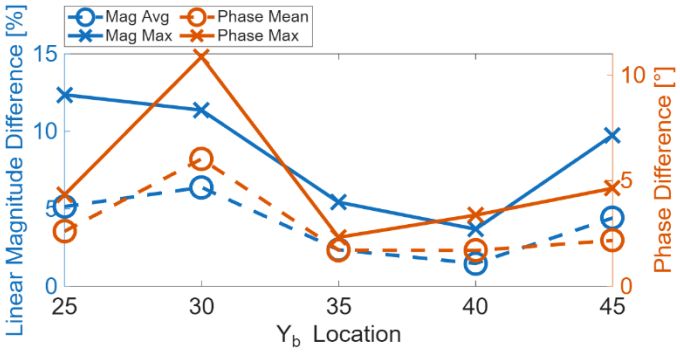

Fig. 9. Full vs empty difference plot of the reflection coefficient for antenna 2 as it sweeps across Y_b while Y_t is held at 75 mm. The average signal at the points of maximum magnitude difference is -30.14 dB, occurring at 3.72 GHz on average The maximum phase differences occur at 3.56 GHz on average.

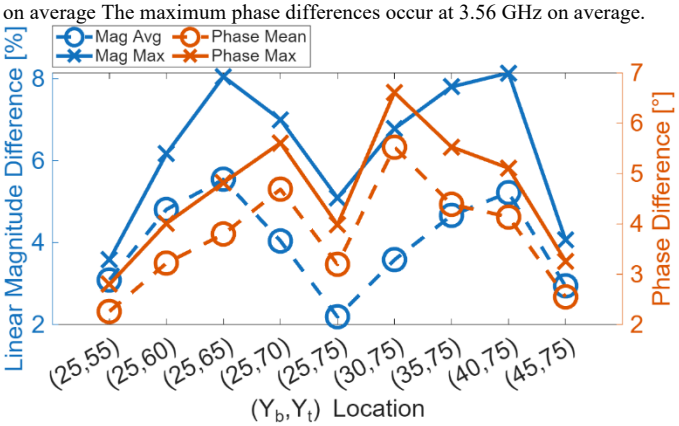

Fig. 10. Full vs empty difference plot of the transmission coefficient between antennas 2 and 5 as they both sweep across Y_b and Y_t. The average signal at the points of maximum magnitude difference is -46.57 dB (higher spacings have lower signal level), occurring at 3.94 GHz on average. The maximum phase differences occur at 3.58 GHz on average.

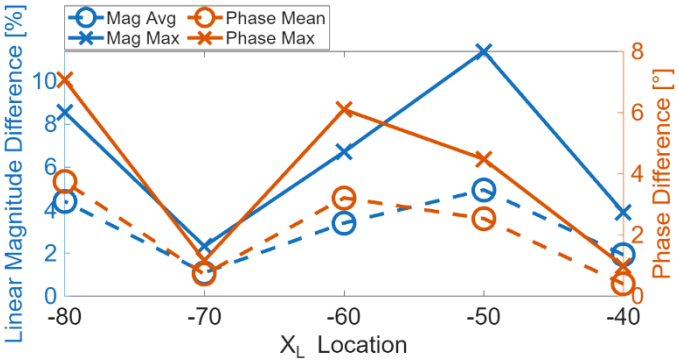

Fig. 11. Full vs empty difference plot of the reflection coefficient for antenna 4 as it sweeps across X_L while X_R is held at 0 mm. The average signal at the points of maximum magnitude difference is -28.53 dB, occurring at 3.7 GHz on average. The maximum phase differences occur at 3.54 GHz on average.

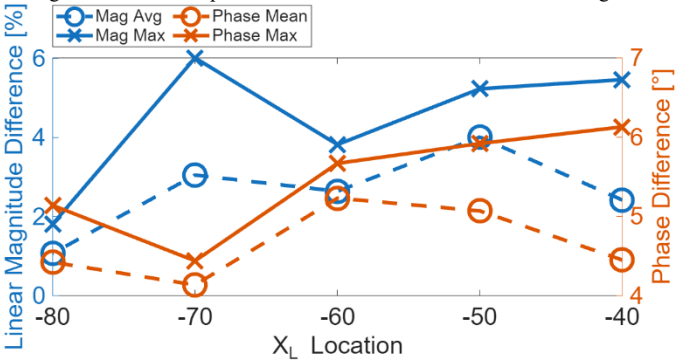

Fig. 12. The full vs empty difference plot of the transmission coefficient between antennas 4 and 5 as antenna 4 sweeps across X_L while X_R is held at 0 mm. The average signal at the points of maximum magnitude difference is -52.87 dB (higher spacings have lower signal level), occurring at 3.89 GHz on average. The maximum phase differences occur at 3.83 GHz on average.

Figs. 11 and 12 show similar results for Scenario 2 as those observed in Scenario 1. Although it is expected that the differences between empty and full for the reflection coefficient of antenna 4 would decrease as it moved away from the bladder, this is not observed. This further suggests that antenna spacing

is at least as important, if not more so, than positioning. This is, of course, relative; spacing becomes irrelevant when the antennas are placed far from the region of interest. A similar trend is shown between the reflection and transmission coefficients, where a high difference in one correlates with low difference in the other. However, this trend does not hold when X_L = -50 mm. The frequency-dependent behaviors for Scenario 2 are consistent with those in Scenario 1.

3) MIC Analysis:

Fig. 13 depicts the MIC matrix comparing the difference between empty and full bladder for each antenna position permutation. It is important to note that these do not simply compare the reflection coefficients or the transmission coefficients individually but consider all the S-Parameters to identify antenna positionings that yield redundant information. This two-element positioning analysis can provide insight into which antenna positions may be redundant or uninformative in the context of imaging or other state determination methods. For Scenario 1, Fig. 13 indicates that the information gained from various permutations is largely similar, with no permutation offering a distinct advantage. Fig. 13 shows that little information is gained when Y_b is swept compared to Y_b = 25 mm or when Y_t is swept compared to Y_t = 75 mm. For Scenario 2, Fig. 13 shows that performing a horizontal sweep of antennas would likely be worthwhile, given the relatively low MIC observed for many vertical spacings. However, with an antenna at position X_L = -50 mm, sweeping may not be necessary or efficient, since additional positions do not provide substantial added information.

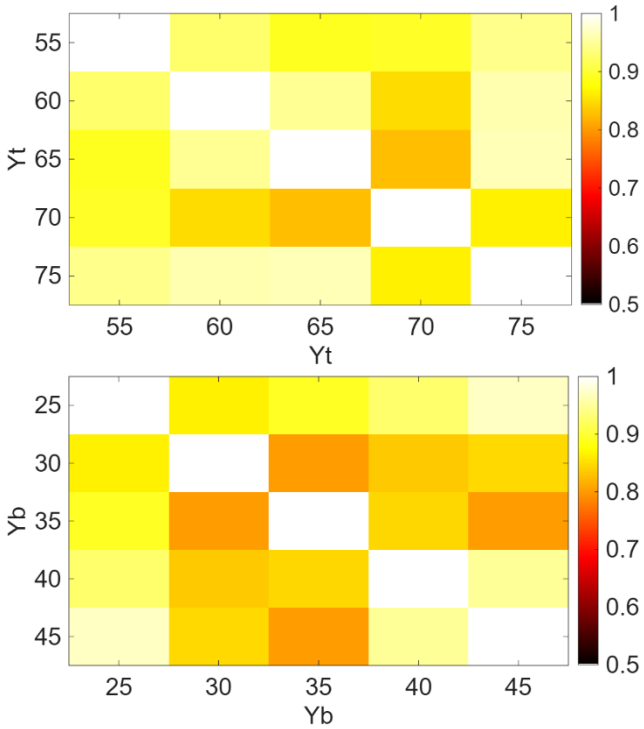

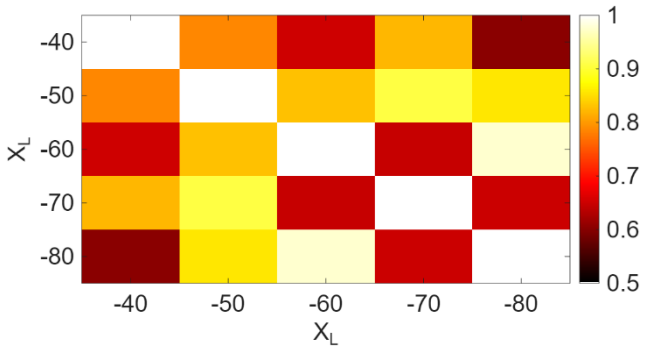

Fig.13. MIC matrices for the signal differences between empty and full in the two-element position study. It includes Scenario 1 with Y_t (top) and Y_b (middle) sweeping and Scenario 2 with X_L sweeping (bottom). The white squares indicate cases where the value does not exist (or is equal to 1). The scale is limited from 0.5 to 1 in order to enhance visual contrast between values.

C. 6-Element Array

1) Full Versus Empty S-Parameter Differences:

Fig. 14 displays a bar graph that shows the maximum linear difference in percent between empty and full for all S-Parameters. The signal level and frequency that the maximum differences occur at is included in a table above Fig. 14. To facilitate practical interpretation of these results, the data is filtered in two ways. In the 'floor filtering', any signal that was below -50 dB at a given frequency was set to -50 dB (estimated as a realistic noise floor). 'Match filtering' was performed by zeroing any signal which had antennas included where the reflection S-Parameters were >-10 dB (i.e., not adequately matched) at a given frequency. 'Full filter' applies both of the above-mentioned constraints. Note that S_{16} and S_{34} are not included in Fig. 14 because no difference across frequency meets both filtering conditions.

Having no floor filter sometimes results in higher differences but with signals 5-10 dB lower than the anticipated noise floor of -50 dB. except for channels S_{16}, S_{46}, S_{34}, and S_{13} which are even lower (up to ~ -100 dB). This indicates that a high SNR system could extract more impactful data from S_{16}, S_{46}, S_{34}, and S_{13}. When the match filtering is not performed, some transmission signals achieve higher differences at lower frequencies around 1.5 GHz. Despite the antennas not being matched at these lower frequencies, the higher penetration depth of the lower frequencies may allow the energy that does go into the body to more easily transmit to the bladder and

reflect to other the other antennas at certain positions.

All reflection parameters have the same maximum difference regardless of filtering method as the lowest reflection signal is about -30.5 dB and the differences occur in the resonance. The transmission parameters see the highest difference when going across the body horizontally (S_{13} and S_{46}) and when going across the body vertically when a center antenna is included (all S-Parameters that include antennas 2 or 5). It is expected that S_{46} has a higher difference than S_{13} due to the empty bladder not being in front of antennas 4 and 6 at all compared to antennas 1 and 3 which will have the empty bladder in front of them. Similar reasoning explains why S_{25} has the highest difference. The center antennas have the most change in bladder, and thus dielectric properties, in their sensing zone as the bladder fills.

2) Microwave Imaging:

Fig. 15 displays 3 images of a full bladder microwave reconstruction at slices from heights of 30 mm, 80 mm, and 140 mm (from the bottom of the model) from left to right respectively. The intensity shown in the color bar is a measure of the contrast in the dielectric properties detected compared to the reference signal by the MW imaging algorithm with a higher number meaning a higher contrast. Fig. 15 serves as an example that the bladder is detected most strongly around the height where it is closest to the skin and shows only noise when looking at the heights in the model where the full bladder is not located. Note that the outline of the bladder is shown on the 80 mm height image slice.

Fig 16. shows an axially-centered slice with the maximum intensities from each height plotted against the depth at which the maximum value occurs. The maximum intensities in Fig. 16 occur close to the center of the bladder in terms of height and at a depth that is inside of the full bladder. The other intensities plotted fall significantly in value when moving outside of the full bladder location. There is an increase in depth around 30 mm – 40 mm which corresponds to the height and depth of the pubic bone at the front of the model. The locations of the antenna and partial outlines of the bladder wall and urine are included in Fig. 16, for reference. Note that the signals used to produce the images in Figs. 15 and 16 were filtered to remove signals below -50 dB.

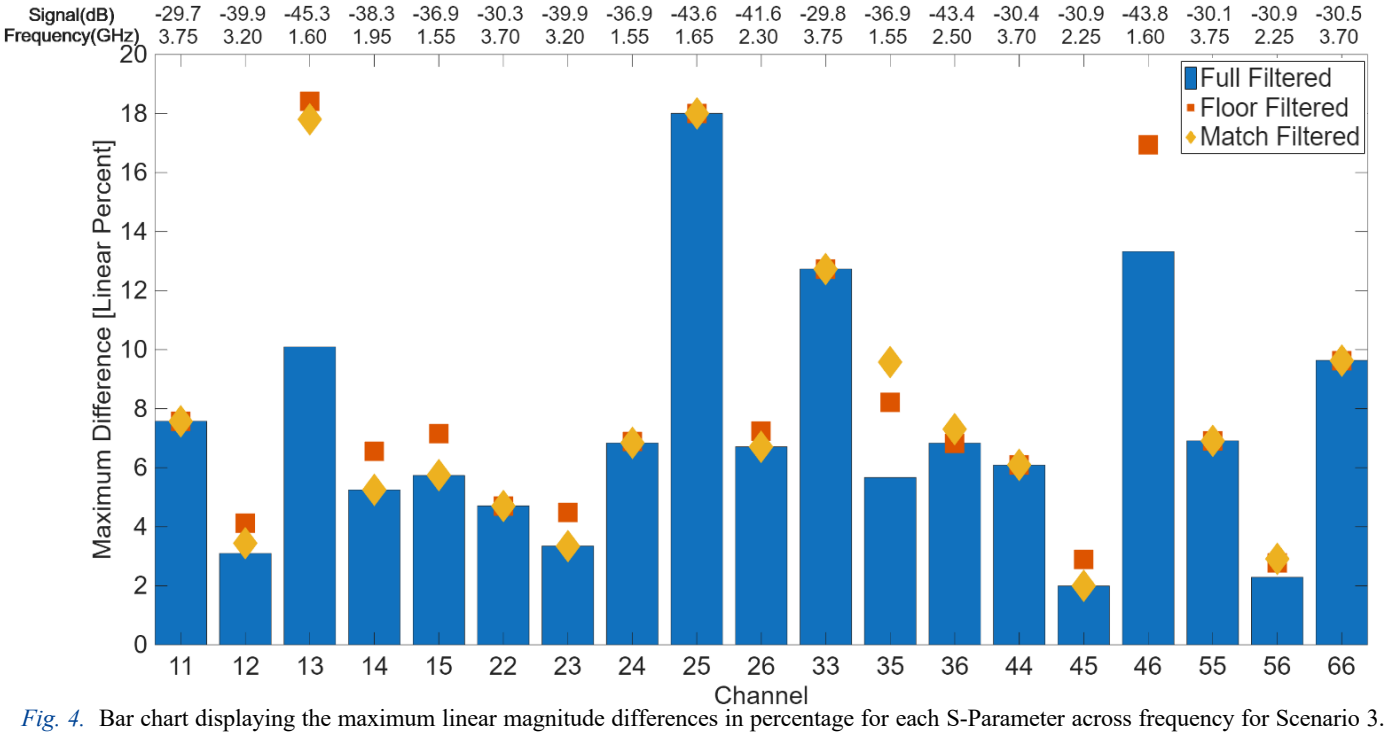

Fig. 4. Bar chart displaying the maximum linear magnitude differences in percentage for each S-Parameter across frequency for Scenario 3. The blue bars ("full filtered") depict the differences when the signal level is limited to >-50 dB and only includes frequencies in the signal where the reflection S-Parameters for each antenna included in the signal is matched (reflection S-Parameters < -10 dB). The floor filtered only includes the -50 dB cut, and the match filtering only includes the matching check of the reflection S-Parameters.

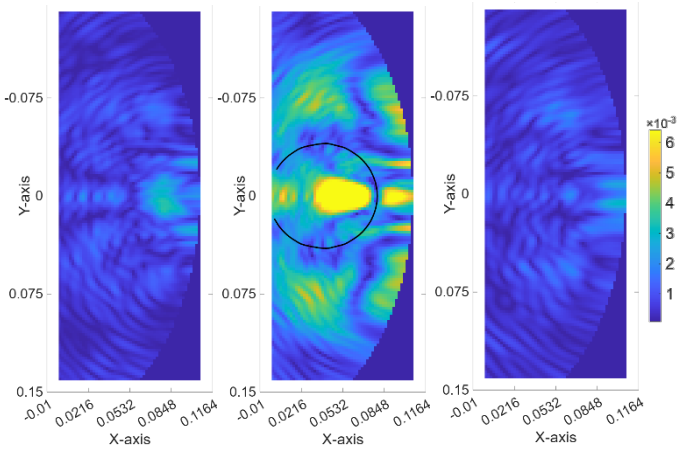

Fig. 5. Three slices from one reconstructed MW image of the full bladder model using the empty bladder model as a reference signal. From left to right, the images, reconstructed using the MERIT algorithm using an average permittivity for the bladder area of 19.72, show slices at heights of 30 mm, 80 mm, and 140 mm. An outline of the bladder is included in the 80 mm height slice.

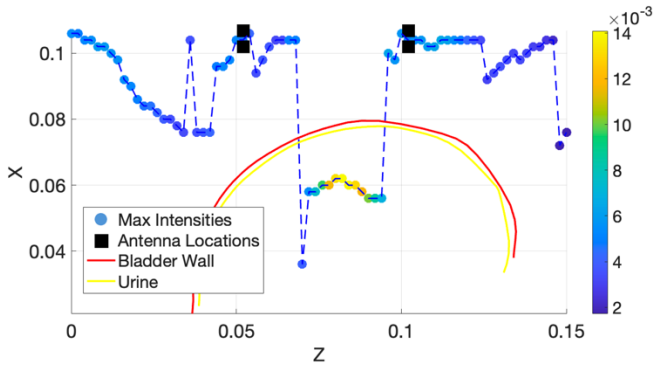

Fig. 6. Side view of maximum intensities from the MW reconstructed images that were calculated at each height of the full bladder model using the empty bladder as a reference. The data is extracted across an axially-centered slice. The height versus depth intensity shows that the highest intensities occur between heights of 80 mm – 90 mm. There is also a notable change in depth located around the 30 mm – 40 mm range which corresponds with the location of the pelvic bone. Antenna, bladder wall, and urine locations are included for reference.

3) *MIC:* Fig. 17 shows the MIC matrix comparing each antenna in the 6-element array in order to determine how much redundant information each antenna provides with respect to other antennas for bladder state detection (full bladder minus empty bladder signals used). This MIC matrix reveals that the most unique information is gained by antennas positioned diagonally to each other followed by the top row antennas providing unique information compared to the bottom row antennas in general. Antennas sharing a row provide a higher level of redundant information with the side antennas in a given row providing highly redundant information. This implies that a similar success of bladder detection could be achieved with 2 antennas removed from the 6-antenna array. Specifically, either antennas 1 and 6 or 3 and 4 should be able to be removed from the array with minimal impact on bladder state detection. This makes sense when considering the width-wise symmetric nature of this area in the body, and this 4-antenna array would cover all unique locations in that respect.

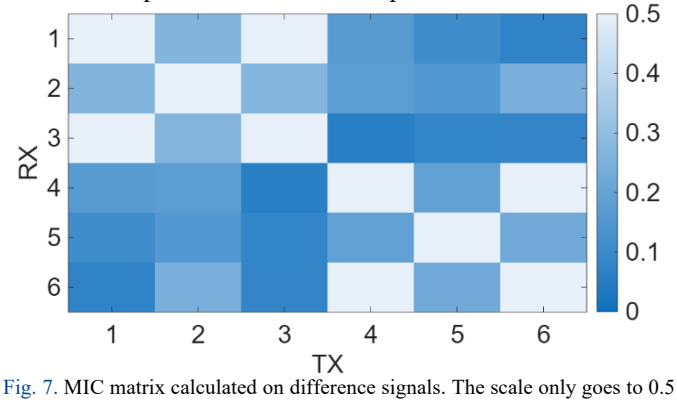

Fig. 7. MIC matrix calculated on difference signals. The scale only goes to 0.5 in order to enhance visibility of the contrast between the lower values in the graph. The MIC values of antenna 1 vs 3 and 4 vs 6 are around 0.85 and appear as 1 (white) in the graph. Diagonal antenna pairings are shown to give highly unique information while across the body (outside edge of array) pairings in the same row provide highly redundant information. Antennas on the bottom row provide unique information compared to the information gained from antennas on the top row.

IV. Discussion and Conclusions

The results presented in this work display a proof of concept for creating a wearable MW array that could be integrated into a bladder monitoring system. Based on the results of the antenna location analysis, it would be recommended that a 4-element array be used with antennas placed above and below the center of the full bladder (likely ¼ of the way up from the hipline to the navel) along with a diagonal pair of antennas next to them (based on optimal antenna spacing). A 2-element array should suffice for bladder state detection as long as 1 antenna is axially centered with respect to the full bladder and that there is a vertical spacing between the two antennas, but 4 is still recommended for robustness to noise. From the frequency analysis, it would be recommended that a lower frequency antenna be used to increase penetration depth. An antenna that operates at 1 GHz, is flexible and conformal, and has broadside radiation would be ideal to incorporate into a wearable MW bladder state detection device. Although lower frequency antennas are larger, it is expected that a 1 GHz design would not be too large to fit comfortably in the target region.

One limitation of this work is that variations of the body model in terms of size, fat-to-muscle ratio, and dielectric properties were not explored and are planned for future studies. It has already been discussed above that a different antenna would be ideal for this application. Future work will address this limitation by designing an antenna tailor made for this application at a lower frequency with higher efficiency and directivity.

Overall, this work can be used as a framework to analyze potential microwave bladder state detection antenna array configurations in the future.

Acknowledgment

We acknowledge the Texas Advanced Computing Center (TACC) at The University of Texas at Austin URL: http://www.tacc.utexas.edu and CMC Microsystems and the Digital Research Alliance of Canada (alliancecan.ca) for providing computing resources that have contributed to the

research results reported within this paper, through solving the Ansys HFSS simulations.

REFERENCES

[1] M. C. Staff, "Urinary incontinence," Mayo Clinic, 9 February 2023. [Online]. Available: https://www.mayoclinic.org/diseases-conditions/urinary-incontinence/symptoms-causes/syc-20352808. [Accessed 15 June 2025].

[2] K. A. Kroeger and R. Sorensen-Burnworth, "Toilet training individuals with autism and other developmental disabilities: A critical review," *Research in Autism Spectrum Disorders,* vol. 3, no. 3, pp. 607-618, 2009.

[3] I. Milsom and M. Gyhagen, "The Prevalence of Urinary Incontinence," *Climacteric: The Journal of the International Menopause Society,* vol. 22, no. 3, pp. 217-222, 2019.

[4] V. M. Drennan and et al., "The prevelance of incontinence in people with cognitive impairment or dementia living at home: A systematic review," *Neurology and Urodynamics,* vol. 32, no. 4, pp. 314-324, 2012.

[5] K. Coyne and et al., "The impact of overactive bladder, incontinence, and other lower urinary tract symptoms on quality of life, work productivity, sexuality, and emotional well-being in men and women: results from the EPIC study," *BJU International,* vol. 101, no. 11, pp. 1388-1395, 2008.

[6] S. Ritblatt and et al., "Parents' and child care professionals'," *Journal of Research in Childhood,* vol. 17, no. 2, pp. 133-146, 2003.

[7] S. W. Leslie, L. N. Tran and Y. Puckett, StatPearls, Treasure Island (FL): StatPearls Publishing, 2024.

[8] E. Porter, A. Raterink and A. Farshkaran, "Microwave-Based Detection of the Bladder State as a Support Tool for Urinary Incontinence [Bioelectromagnetics]," *IEEE Antennas and Propagation Magazine,* vol. 64, no. 1, pp. 112-122, 2022.

[9] M. Tim Newman (Medically Reviewed by Roger Bielinski, "What to know about urinary incontinence," Medical News Today, 31 March 2025. [Online]. Available: https://www.medicalnewstoday.com/articles/165408. [Accessed 15 June 2025].

[10] J. L. Matson and S. LoVullo, "Encopresis, soiling and constipation in children and adults with," *Res. Dev. Disabil,* vol. 30, no. 4, pp. 799-807, 2009.

[11] L. E. Smith, M. J. Maenner and M. M. Seltzer, "Developmental Trajectories in Adolescents and Adults," *Journal of the American Academy of Child & Adolescent,* vol. 51, no. 6, pp. 622-631, 2012.

[12] M. Maenner and et al., "Prevalence of Autism Spectrum Disorder Among Children Aged 8 Years - Autism and Developmental Disabilities Monitoring Network, 11 Sites, United States, 2016," *MMWR Surveill. Summ,* vol. 69, no. 4, pp. 1-12, 2020.

[13] M. J. Maenner and et al., "Prevalence and Characteristics of Autism Spectrum Disorder Among Children Aged 8 Years - Autism and Developmental Disabilities Monitoring Network, 11 Sites, United States, 2018," *MMWR Surveillance Summary,* vol. 70, no. 11, pp. 1-16, 2021.

[14] CDC NCHS Data Brief No. 291, "Estimated Prevalence of Children With Diagnosed Developmental Disabilities in the United States, 2014-2016," CDC, 2017.

[15] L. Levato and et al., "Use of urine alarms in toilet training children with intellectual and developmental disabilities," *Research in Developmental Disabilities,* Vols. 53-54, pp. 232-241, 2016.

[16] L. A. LeBlanc and et al., "Intensive outpatient behavioral treatment of primary urinary incontinence of children with autism," *Focus on Autism and Other Developmental Disabilities,* vol. 20, pp. 98-105, 2005.

[17] N. M. Hanney and et al., "Intensive behavioral treatment of urinary incontinence of children with autism spectrum disorders: An archival analysis of procedures and outcomes from an outpatient clinic," *Focus on Autism and Other Developmental Disabilities,* vol. 28, no. 1, pp. 26-31, 2012.

[18] K. A. Kroeger and R. Rorensen-Burnworth, "Toilet training individuals with autism and other developmental disabilities: A critical review," *Research in Autism Spectrum Disorders,* vol. 3, no. 3, pp. 607-618, 2009.

[19] E. Van Laecke, *Approach to refractory urinary incontinence in children, with special emphasis on children with intellectual and/or physical disability,* Ph.D. Thesis: Faculty of Medicine and Health Sciences, Paediatric Urology, Department of Urology, Ghent University, 2009.

[20] J. L. Matson, "Tehcnology Used in Toilet Training," in *Clinical guide to toilet training children*, Springer International Publishing/Springer Nature, 2017, pp. 169-180.

[21] J. G. Forsberg, "A morphologist's approach to the vagina: Age-related changes and estrogen sensitivity," *Maturitas,* vol. 22, pp. 7-15, 1995.

[22] T. A. Shamliyan and et al., "Systematic Review: Randomized, Controlled Trials of Nonsurgical Treatments for Urinary Incontinence in Women," *Annals of Internal Medicine,* vol. 148, no. 6, 2008.

[23] M. Sanantonio and et al., "The Impact of Hands on Education, Quality Incontinence Briefs and Wipes in Sub-Acute/LTC Facilities Study Overview," WoundSource, 26 September 2019. [Online]. Available: https://www.woundsource.com/blog/impact-hands-education-quality-incontinence-briefs-and-wipes-in-sub-acuteltc-facilities-study. [Accessed 15 June 2025].

[24] MedlinePlus, "Skin care and incontinence," A.D.A.M Inc., 15 February 2024. [Online]. Available: https://medlineplus.gov/ency/article/003976.htm. [Accessed 15 June 2025].

[25] A. Hafid and et al., "State of the Art of Non-Invasive Technologies for Bladder Monitoring: A Scoping Review," *Sensors,* vol. 23, no. 5, p. 2758, 2023.

[26] Novioscan, "Products," 2025. [Online]. Available: https://novioscan.com/products. [Accessed 15 June 2025].

[27] P. G. Van Leuteren, A. J. Nieuwhof-Leppink and P. Dik, "SENS-U: clinical evaluation of a full-bladder notification - a pilot study," *Journal of Pediatric Urology,* vol. 15, no. 4, pp. 381.1-381.5, 2019.

[28] A. J. Macnab and et al., "Simultaneous functional near infrared spectroscopy of the brain and bladder," in *Proc. SPIE 11237, Biophotonics in Exercise Science, Sports Medicine, Health Monitoring Technologies, and Wearables, 112370T*, 2020.

[29] E. Pancera and et al., "Ultra-wideband radar imaging: An approach to monitor the water accumulation in the human body," in *IEEE International Conference on Wireless Information Technology and Systems*, Honolulu, Hawaii, USA, 2010.

[30] A. Farshkaran and et al., "Proof of Concept of Microwave-Based Bladder State Detection Using Realistic Pelvic Models," *IEEE Open Journal of Engineering in Medicine and Biology,* vol. 5, pp. 140-147, 2024.

[31] World Health Organization (WHO), "Electromagnetic Fields (300 Hz to 300 GHz), Environmental Health Criteria 137," Geneva, Switzerland, 1993.

[32] International Commission on Non-Ionizing Radiation Protection (ICNIRP), "Exposure to high frequency electromagnetic fields, biological effects and health consequences (100 kHz-300 GHz)," Munich, Germany, 2009.

[33] Institute of Electrical and Electronic Engineers (IEEE), "IEEE C95.1-2005 Standard for Safety Levels with Respect to Human Exposure to Radio Frequency Electromagnetic Fields, 3 kHz to 300 GHz," New York, USA, 2005.

[34] Federal Communications Commissions, "FCC Policy on Human Exposure to Radio Frequency Electromagnetic Fields," 1996.

[35] M. O'Halloran and et al., "Ultra wideband radar system for bladder monitoring applications," *Prog. Electromagn. Res. C,* vol. 33, pp. 17-28, 2012.

[36] F. Krewer and et al., "Development of a wearable microwave bladder monitor for the management and treatment of urinary incontinence," in *Proc. SPIE Defense + Security*, Baltimore, MD, USA, 2014.

[37] E. Pancera and et al., "Ultra wideband radar imaging: An approach to monitor the water accumulation in the human body," in *Proc. IEEE Int. Conf. Wireless Inf. Technol. Syst.*, Honolulu, HI, USA, 2010.

[38] J. Schmid and et al., "Ultra-wideband signals for the detection of water accumulations in the human body," in *Proc. Int. Conf. Bio-inspired Syst. Signal Process*, Valencia, Spain, 2010.

[39] X. Li and et al., "Performance of an ultra wideband radar for detection of water accumulation in the human bladder," in *Proc. 7th Eur. Radar Conf.*, Paris, France, 2010.

[40] X. Li and et al., "Ultra wideband radar for water detection in the human body," in *German Microwave Conf. Dig. Papers*, Berlin, Germany, 2010.

[41] X. Li and et al., "Synthetic aperture-based UWB imaging system for detection of urine accumulation in human bladder," in *Proc. IEEE Int. Conf. Ultra-Wideband (ICUWB)*, Bologna, Italy, 2011.

[42] X. Li and et al., "Array configurations of a UWB near field imaging system for the detection of water accumulation in human body," in *Proc. 8th Eur. Radar Conf.*, Manchester, U.K., 2011.

[43] M. O'Halloran and et al., "Bladder-state monitoring using ultra wideband radar," in *Proc. 7th Eur. Conf. Antennas Propag. (EuCAP)*, Gothenburg, Sweden, 2013.

[44] A. Fry and et al., "Microwave Bladder Monitoring: Analysis of 3x2 Array and Impact of Antenna Location," in *IEEE International Symposium on Antennas & Propagation and North American Radio Science Meeting*, Ottawa, Canada, 2025.

s[45] C. Baumgartner and et al., "IT'IS Database for thermal and electromagnetic parameters of biological tissues - Ver. 4.2," IT'IS Foundation, April 2024. [Online]. Available: itis.swiss/database.

[46] S. Nishikori and S. Fujita, "Association of fat-to-muscle mass ratio with physical activity and dietary protein, carbohydrate, sodium, and fiber intake in a cross-sectional study," *Scientific Reports,* vol. 14, no. 1, 2024.

[47] A. Farshkaran and E. Porter, "Importance of Sex-Based Modelling of the Pelvic Region for Microwave Medical Applications," in *IEEE MTT-S International Microwave Bio Conference (IMBioC)*, Suzhou, China, 2022.

[48] E. Pancera and et al., "Performance of ultra wideband antennas for monitoring water accumulation in human bodies," in *Proc. 4th Eur. Conf. Antennas Propag. (EUCAP)*, Barcelona, Spain, 2010.

[49] M. Wang, L. Crocco and M. Cavagnaro, "On the Design of a Microwave Imaging System to Monitor Thermal Ablation of Liver Tumors," *IEEE Journal of Electromagnetics, RF, and Microwaves in Medicine and Biology,* vol. 5, no. 3, pp. 231-237, 2021.

[50] M. Wang and et al., "A Compact Slot-Loaded Antipodal Vivaldi Antenna for a Microwave Imaging System to Monitor Liver Microwave Thermal Ablation," *IEEE Open Journal of Antennas and Propagation,* vol. 3, pp. 700-708, 2022.

[51] H. Bahramiabarghouei and et al., "Flexible 16 Antenna Array for Microwave Breast Cancer Detection," *IEEE Transactions on Biomedical Engineering,* vol. 62, no. 10, pp. 2516-2525, 2015.

[52] Y. M. Abbosh and et al., "Non-Uniform Antenna Array for Enhanced Medical Microwave Imaging," *Sensors,* vol. 25, no. 10, 2025.

[53] D. O'Loughlin, "Open-source software for microwave radar-based image reconstruction," in *Proc. Eur. Conf. Antennas Propag*, 2018.